AIChE

Multiscale Dynamic Monte Carlo/Continuum Model of Drying and Nonideal Polycondensation in Sol-Gel Silica Films

Xin Li and Stephen E. Rankin
Dept. of Chemical and Materials Engineering, University of Kentucky, Lexington, KY 40506

DOI 10.1002/aic.12202
Published online March 10, 2010 in Wiley Online Library (wileyonlinelibrary.com).

The process of forming sol-gel silica thin films involves multiple length and time scales ranging from molecular to macroscopic, and it is challenging to fully model because the polymerization is nonideal. A multiscale model is described to link macroscopic flow and drying (controlled by process parameters) to film microstructure (which dictates the properties of the films). In this modeling strategy, dynamic Monte Carlo (DMC) polymerization simulations are coupled to a continuum model of drying. The entire DMC simulation is treated as a particle of sol whose position and composition are tracked using a diffusion/evaporation finite difference method. By simulating swarms of particles starting from different positions in the film, the multiscale model predicts different drying/gelation phenomena, and predicts the occurrence of gradients of concentration and gelation in the films which can lead to the formation of a gel skin near the top surface of the film. © 2010 American Institute of Chemical Engineers *AIChE J,* 56: 2946–2956, 2010

Keywords: multiscale modeling, sol-gel silica films, dynamic Monte Carlo, polycondensation, first shell substitution effect

Introduction

Sol-gel silica films are of sustained and growing interest as engineered materials for a variety of applications,[1–3] e.g., sensor concentrators,[4–10] optical materials,[11–14] electrical insulators,[15] and solar energy applications.[16] In sol-gel film processing, a continuous liquid phase displaces air at the substrate through a wetting process and undergoes a process of drying and polycondensation to form a stable porous film.[17,18] Modeling silica curing in drying films is important for understanding the development of microstructure in the films and for overcoming challenges in controlling the thickness, cracking, and homogeneity. Until now, most models of sol-gel polymerization or drying polymer films have provided useful insights into the essence of the physical phenomena, but they only focused on selected length and time scales. For example, kinetic models of the gelation behavior of silica polymerization have been developed using recursive statistical technique or Monte Carlo simulation.[19–22] These modeling approaches are necessary to link rates of polymerization of individual monomers to molecular weight distributions and gelation of branched polymers. On the other hand, drying has been approached using continuum models and solved with an integral approach,[23] finite element method,[24–26] or finite difference method.[27–30] However, during the formation of sol-gel coatings, both polymerization and drying occur simultaneously, so the process involves multiple length and time scales ranging from molecular to macroscopic.

Multiscale modeling techniques have developed rapidly in recent years due to both advances in computer processing power and the recognition of the importance of treating multiple length scales in biological and materials systems.[31,32] Unlike other processes where multiscale models have previously been applied, the sol-gel polycondensation occurs throughout the thickness of the film where solvent transport is occurring. Therefore, it is not possible to regard the

Correspondence concerning this article should be addressed to S. E. Rankin at srankin@engr.uky.edu.
Current Address of Xin Li: Medical College of Wisconsin, Milwaukee, WI.

polymerization reaction as occurring in a place spatially separate from the place where the coating flow occurs, as has been done for catalytic and thin film deposition processes.[33–37] At the molecular level, polymerization and (if surfactants are added) self-assembly processes occur, which control the film properties such as film microstructure. At the same time, the formation of the film is controlled by macroscopic parameters. Diffusion and mass transport occur over micron or greater length scales, and define the concentration fields within which polymerization and self-assembly occur. Therefore, we are challenged in this process to develop a methodology to link different length and time scales together throughout the entire simulated domain.

Here we present a multiscale model, which captures the evolution of both macroscopic and molecular phenomena during the sol-gel silica film formation process. The process of diffusion and mass transport can be adequately modeled by treating the film as a continuum.[38] The macroscopic conservation equations for mass are expressed by a set of partial differential equations for species concentration with initial and boundary conditions. Using the finite difference method, the continuous domain is discretized and these PDEs are solved numerically. However, at the molecular length scale, the continuum hypothesis is no longer valid and the molecular phenomena cannot be described by deterministic PDEs.[39] At such a small length scale, the kinetics of sol-gel polymerization is best modeled by dynamic Monte Carlo (DMC) simulation. This approach is necessary because of the nonideal nature of silane polymerization (which precludes the use of random branching theory[40–42] and even throws into question the validity of statistical techniques such as the kinetic-recursive method[20,21]). DMC simulations can simulate much longer times and much larger ensembles than molecular dynamics simulations,[19,43] and they have the potential flexibility to handle large cycles and cages that are thought to play a significant role in the structure of sol-gel silica.[19,44,45] The inclusion of these cyclization reactions will be described in future contributions from our group.

Here, we describe the methodology required to integrate a DMC model of nonideal, branched polycondensation and a continuum model of drying. This model extends the 1D continuum drying/curing model of Cairncross et al.[38] by using the DMC method to predict polymer structure distributions rather than a statistical recursive approach. We begin by describing the multiscale model, including the physical assumptions and the simulation procedure. As part of the description of the DMC model, the sol-gel silicate kinetics is reviewed. Details are given about methods to calculate the conversion, time interval, gel point, and other properties of the evolving population of silicate oligomers in the DMC model. In the continuum model, the entire DMC simulation (containing $\sim 2.5 \times 10^6$ monomers) is treated as a particle of sol whose position and composition are tracked using diffusion/evaporation finite difference calculations. Linking the two models is accomplished by tracking the positions of sol particles during drying and using concentration of that sol particle to provide a "handshake" (a common variable between model components with different scales) between the continuum calculation and the DMC model. The other "handshake" between the two models comes from using calculated time steps from the DMC model as the time intervals for the continuum calculation to synchronize both parts of the simulation method. Here, two specific polycondensation cases are considered—ideal polymerization and polymerization with a first shell substitution effect (FSSE) consistent with prior NMR experiments. The effects of concentration gradients during drying are captured by simulating swarms of particles starting from different positions in the film. By varying process parameters represented in dimensionless form with a combination of Biot and Damköhler numbers, we observe their effects on the competition between drying and gelation, predict different drying/gelation phenomena, and predict the occurrence of gradients of concentration and gelation in the films, which can lead to the formation of a gel skin near the top surface of the film.

Modeling

Sol-gel silicate kinetics

Under acid-catalyzed conditions, silicon alkoxide molecules react through hydrolysis and condensation reactions to ultimately produce a homogeneous gel. The functional-group reactions are illustrated by Eqs. 1–3[46,47] for individual silicon "sites," which we define to be a silicon atom identified by the number of alkoxide, hydroxide, and siloxane groups attached.

Hydrolysis:

$$\equiv\text{Si}\text{—}\text{OR} + \text{H}_2\text{O} \overset{K_h}{\longleftrightarrow} \equiv\text{Si}\text{—}\text{OH} + \text{ROH} \quad (1)$$

Water-producing condensation:

$$\equiv\text{Si}\text{—}\text{OH} + \text{HO}\text{—}\text{Si}\equiv \rightarrow \equiv\text{Si}\text{—}\text{O}\text{—}\text{Si}\equiv + \text{H}_2\text{O} \quad (2)$$

Alcohol-producing condensation:

$$\equiv\text{Si}\text{—}\text{OR} + \text{HO}\text{—}\text{Si}\equiv \rightarrow \equiv\text{Si}\text{—}\text{O}\text{—}\text{Si}\equiv + \text{ROH} \quad (3)$$

In general, the rates of these reactions depend at least on the identities of the four other moieties attached to the silicon atom, which gives rise to a complex kinetic modeling problem with multiple FSSEs.[48] However, experiments have shown that under acidic conditions, the hydrolysis rate coefficients can be at least an order of magnitude larger than the condensation rate coefficients, so hydrolysis can be modeled by assuming that it reaches quasi-equilibrium.[49–51] This equilibrium condition allows one to characterize hydrolysis using only the average hydrolysis extent χ[52]:

$$\chi = \frac{[\equiv\text{SiOH}]}{[\equiv\text{SiOH}] + [\equiv\text{SiOR}]}. \quad (4)$$

Because hydrolysis equilibrium coefficients are all similar regardless of substitution, it is possible to regard χ as a constant for all silicon sites.[51] Also, if the amount of water is sufficient, χ can be regarded as constant with respect to time as well.[49]

Based on the fact that there is a strong, negative first shell substitution effect (FSSE) in the condensation reactions under acidic conditions,[49,53] and by assuming that water-producing condensation (Eq. 2) dominates over alcohol-

producing condensation (Eq. 3),[46,47] the set of bimolecular condensation can be written as:

$$Q_i + Q_j \xrightarrow{k_{ij}^*} Q_{i+1} + Q_{j+1} + H_2O, \tag{5}$$

where Q_i represents a tetrafunctional silicon site with i siloxane bonds (i.e., i represents the number of linkages to other silicon atoms), and both i and j can vary between 0 and 3.[19] Assuming that hydrolysis reaches quasi-equilibrium with constant χ, the rate of reaction in Eq. 5 can be expressed as:

$$R_{ij}^{\text{bimol}} = \begin{cases} \chi^2(f-i)(f-j)k_{ij}[Q_i][Q_j], & i \neq j \\ \frac{1}{2}\chi^2(f-i)(f-j)k_{ij}[Q_i][Q_j], & i = j \end{cases} \tag{6}$$

where k_{ij} is the rate constant of bimolecular polycondensation (defined as reactivity per unit of silanol concentration), f is the functionality of the monomer (which is equal to 4 here), and $[Q_i]$ represents the concentration of silicon sites Q_i,[21] which is defined in the DMC simulation as follows:

$$[Q_i] = \frac{N_{Q_i}}{N_A \times V}, \tag{7}$$

where N_{Q_i} is the number of silicon site Q_i, N_A is the Avogadro number ($6.022\text{E} + 23\ \text{mol}^{-1}$), and V is the volume of the DMC simulation.

DMC model

The DMC model is solved based on the following assumptions: Only a first shell substitution effect for condensation is considered, hydrolysis is assumed to be at quasi-equilibrium, alcohol-producing condensation is neglected, and no cyclization is allowed. With this set of assumptions, a finite set of N monomers ($N \sim 2.5 \times 10^6$) is polymerized in a manner consistent with the kinetics described above by a continuous-time DMC approach.[43,54]

In the simulation, each monomer unit is indexed as a separate entity. We need to record a great deal of information about the progress of the polycondensation process, such as the populations of silicon sites with different degrees of condensation, molecular tags providing a unique identity for each molecule, the sizes of molecules, and the molecule membership of the silicon sites. At each DMC step, two (SiOH) functional groups react to form one siloxane bond (SiOSi), and the conversion (α) is increased by a small constant value $\Delta\alpha$. Because the total number of (SiOH) groups present at the start of the simulation is four times the number of silicon sites, $\Delta\alpha$ is given by:

$$\Delta\alpha = \frac{2}{4 \times N} = \frac{1}{2N} = 2.0 \times 10^{-7}. \tag{8}$$

Therefore, the cumulative conversion can be calculated as

$$\alpha = \frac{[\text{SiOSi}]}{4[\text{Si}]} = \frac{2 \times S_t}{4 \times N}, \tag{9}$$

where S_t is the total number of DMC steps and N is the total number of silicon sites.

At each step, the probabilities P_{ij} of selecting each type of condensation reaction are evaluated by calculating the rates of the reactions, and one reaction is chosen to occur. To simplify the calculation, the set of numbers of silicon sites, N_{Qi}, are used rather than $[Q_i]$ to give $R_{ij}^{\text{bimol}*} = (N_A V)^2 R_{ij}^{\text{bimol}}$. The probabilities are normalized using the sum of all reaction rates ($P_{ij} = R_{ij}^{\text{bimol}*} / \sum_{j \geq i} R_{ij}^{\text{bimol}*}$), and a random number is used to select the reaction that occurs. This Monte Carlo reaction selection method ensures the proper competition among reactions.[55] After selecting a reaction, the particular sites joined by the reaction are randomly chosen from the subset of sites fitting to the required characteristics—In this case, that the sites have the correct connectivities for the selected reaction. After the sites are chosen, they are joined with one siloxane bond and all information is updated. DMC steps are repeated until a stopping criterion is met based on the desired information to be obtained from the model—Usually by the point that the weight average degree of polymerization DP_w (see below) reaches at most 10% of the total number of sites (N).

In addition to the conversion evolving during each Monte Carlo step, the time interval[43,54] is also calculated according to the "continuous time" approach initially described by Gillespie. Briefly, this can be derived starting from the expression for the average rate of change of conversion, $d\alpha/dt = d\left(\sum i[Q_i]/4[Q_0]_0\right)/dt$. Using the relations $[Q_0]_0 = C_{\text{Si}} = \text{constant}$, $d(\sum i[Q_i])/dt = 2\sum R_{ij}^{\text{bimol}}$ and assuming that, for a small increment of α, that $d\alpha/dt = \Delta\alpha/\Delta t$, one can derive the following expression based on the approach of Gillespie[54]:

$$\Delta t = \frac{C_{\text{Si}}}{N \sum R_{ij}^{\text{bimol}}} \ln\left(\frac{1}{r}\right) = \frac{N}{C_{\text{Si}} \sum R_{ij}^{\text{bimol}*}} \ln\left(\frac{1}{r}\right), \tag{10}$$

where N is the total number of silicon sites, r is a random number from (0, 1), and C_{Si} is the total silicon site concentration which comes from the continuum model at the time that the reaction is selected (see later). This concentration serves as one link that allows us to correlate the DMC model and the continuum model in this multiscale process. We will give more details in the following description of the continuum model.

One of the important results we need to obtain from the DMC simulation is the gel point. We know that a gel is a sample-spanning polymer network. In theory, we can use an infinite molecular weight polymer to represent the gel.[20] In the DMC simulation, the gel point can be estimated by the point at which DP_w appears to begin to diverge (although it will not truly diverge because of the finite population of monomers), or even more accurately by a maximum in the value of $r\text{DP}_w$.[19,21] DP_w is the weight-averaged degree of polymerization, and $r\text{DP}_w$ is the reduced weight-averaged degree of polymerization, which is calculated by removing the largest molecule (which after the gel point is the gel itself) from the population and recalculating DP_w.

$$\text{DP}_w = \frac{1}{N}\sum_{i=1}^{N_{\text{mol}}} L(i)^2, \tag{11}$$

$$r\text{DP}_w = \frac{\sum_{i=1}^{N_{\text{mol}}} L(i)^2 - (L_{\max})^2}{N - L_{\max}}, \tag{12}$$

where N_{mol} is the number of molecules, $L(i)$ is the size of molecule with tag i and $L_{\max}$ is the size of the largest molecule in the population.

Here, we will simulate two cases with the DMC model—An ideal polycondensation case and a FSSE case. In the ideal polycondensation case, the functional groups are assumed to react randomly and independently, which means that all the rate constants are equal to each other and no cyclization is allowed to happen. In the FSSE case, we consider nonideal polymerization effects, but still exclude cyclization. The rate coefficients of the FSSE case are set to drop by 10% across each row in the matrix of bimolecular rate coefficients used in Eq. 6 and to decrease by 90% down the diagonal, which resembles the experimental substitution effect.[19] In other words, $k_{01} = 0.9k_{00}$, $k_{02} = 0.81k_{00}$, etc., whereas $k_{11} = 0.1k_{00}$, $k_{22} = 0.01k_{00}$, etc. In fact, the ideal case represents a particular case of the FSSE model in which the set of connectivity-dependent rate coefficients are all set equal to one another ($k_{00} = k_{01} = k_{02} = k_{11} = k_{12} = \ldots$).

Continuum drying model

Model Assumptions and Description. The loss of solvent by evaporation from sol-gel thin-film coatings is described by macroscopic conservation of mass equations. Here we use a simplified one-dimensional model corresponding to a rapidly deposited film that begins drying and curing after the coating process is complete. Solvent leaves continuously by evaporation at the upper liquid/vapor interface. In addition to this evaporation, the diffusion of solvent within the film and the chemical reactions of dissolved species need to be included in this model. A schematic diagram of the sol-gel film drying process is presented in Figure 1.

To facilitate the modeling, the following primary assumptions are made:

1) The film is extremely thin as compared with the surface area so that concentration variation is assumed to occur only in the thickness direction.

2) The concentrations of species are uniform throughout the film at the beginning of the drying process.

3) The solid substrate supporting the thin film is taken to be impermeable.

4) At the surface of the coating the vapor is in equilibrium with the coating, and the pressure in the gas phase is effectively uniform.

5) The evaporation rate of the solvent from the surface is proportional to the difference in gas-phase mole fraction of solvent between the vapor just above the surface of the film and the bulk gas.

6) The process is isothermal, i.e., heat transfer effects are not considered here. This is reasonable because of the slow rate of silica polycondensation but could be corrected by adding energy conservation equations.[25]

7) The diffusion coefficients of solvent and sol are assumed to be constant and equal, and the cross-term diffusion coefficients are set to zero.

8) Hydrolysis is assumed to achieve quasi-equilibrium before the drying process is started with hydrolysis extent $\chi = 1$.

9) Alcohol has already evaporated before the drying process is started and there is excess water in the solution. That means we can consider just water as the solvent.

10) The film thickness changes are assumed to be dominated by solvent evaporation so that volume changes due to reactions can be ignored.

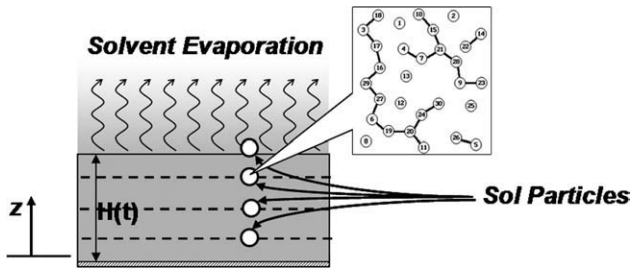

Figure 1. Schematic of the 1-D drying model of sol-gel silica.

The z direction is defined to be perpendicular to the drying film. The initial thickness of the film is H_0, and during the drying process, the instantaneous thickness is $H(t)$. The entire DMC simulation (containing millions of monomers) is treated as a particle of sol whose position and composition are tracked using a diffusion/evaporation finite difference calculation.

Governing Equations. Based on the above assumptions, the governing equations for solvent and solute are as follows:

$$\frac{\partial C_1}{\partial t} - D_1 \frac{\partial^2 C_1}{\partial z^2} = 0 \tag{13}$$

$$\frac{\partial C_2}{\partial t} - D_2 \frac{\partial^2 C_2}{\partial z^2} = 0 \tag{14}$$

$$\frac{\partial Q_i^{\mathrm{C}}}{\partial t} - D_{Q_i^{\mathrm{C}}} \frac{\partial^2 Q_i^{\mathrm{C}}}{\partial z^2} = R_{Q_i^{\mathrm{C}}} (i = 0, 1, 2, 3, \text{ and } 4) \tag{15}$$

where C_1 is the concentration of solvent, C_2 is the total silicon concentration, Q_i^{C} is the concentration of a tetrafunctional silicon site with i siloxane bonds in the continuum model. The relationship between C_2 and Q_i^{C} is $\mathrm{C}_2 = \sum_{i=0}^{4} Q_i^{\mathrm{C}}$. $R_{Q_i^{\mathrm{C}}}$ is the net rate for creation of each type of site through reaction.

$$R_{Q_i^{\mathrm{C}}} = \sum_{j=0}^{3} R_{(i-1)j} - \sum_{j=0}^{3} R_{ij} (i = 0, 1, 2, 3, \text{and } 4) \tag{16}$$

where R_{ij} is the bimolecular reaction rate between sites Q_i and Q_j given by Eq. 6.

Initial conditions in this formulation are as follows:

$$C_1(0, z) = C_{1,0}; \quad C_2(0, z) = C_{2,0}; \quad Q_i^{\mathrm{C}}(0, z) = Q_{i,0}^{\mathrm{C}} (i = 0, \ 1, 2, 3, \text{and } 4). \tag{17}$$

Consistent with the description of the film model described above, the boundary conditions are given by:

At the substrate ($z = 0$):

$$D_i \frac{\partial C_i}{\partial z} = 0 \quad (i = 1, 2) \tag{18}$$

$$D_{Q_i^{\mathrm{C}}} \frac{\partial Q_i^{\mathrm{C}}}{\partial z} = 0 \quad (i = 0, 1, 2, 3, \text{and } 4) \tag{19}$$

At the free surface ($z = h(t)$):

$$-D_1\frac{\partial C_1}{\partial z} - C_1\frac{dH(t)}{dt} = k_g(y_1^s - y_1^\infty) \tag{20}$$

$$\frac{\partial C_2}{\partial z} = -\frac{\hat{V}_1}{\hat{V}_2}\frac{\partial C_1}{\partial z} \tag{21}$$

$$\frac{\partial Q_i^C}{\partial z} = \frac{Q_i^C}{C_2}\frac{\partial C_2}{\partial z} \tag{22}$$

The effect of boundary motion due to solvent evaporation is taken into account using the term $\frac{dH(t)}{dt}$.[56] In Eq. 20, k_g is the mass transfer coefficient of solvent in the vapor phase, y_1^s is the molar fraction of solvent at the surface in the gas phase (which is calculated based on Raoult's law), and y_1^∞ is the molar fraction of solvent far away in the gas, which is set to zero here. Equation 21 was derived from the relation $C_1\hat{V}_1 + C_2\hat{V}_2 = 1$, where $\hat{V}_i$ is the molar volume, and $\hat{V}_2 = \frac{1-C_{1,0}\hat{V}_1}{C_{2,0}}$. Equation 22 is obtained by recognizing that the probability that a Si atom in the solute mixture is associated with a Q_i^C site is given by Q_i^C/C_2. Using this relationship, the diffusion term for Q_i^C can also be substituted into Eq. 15 as follows:

$$D_{Q_i^C}\frac{\partial^2 Q_i^C}{\partial z^2} = \frac{Q_i^C}{C_2}D_2\frac{\partial^2 C_2}{\partial z^2}, \tag{23}$$

and so

$$\frac{\partial Q_i^C}{\partial t} - \frac{Q_i^C}{C_2}D_2\frac{\partial^2 C_2}{\partial z^2} = R_{Q_i^C}. \tag{24}$$

Because only solvent is assumed to evaporate, the rate of change of film thickness, also known as the surface velocity v^s, can be calculated according to the following expression:

$$\frac{dH(t)}{dt} = v^s = -\hat{V}_1 k_g(y_1^s - y_1^\infty). \tag{25}$$

To confirm the accuracy of our multiscale implementation, we can write balance equations for reactive silanol species. For ideal polycondensation, the model can be simplified because the condensation rate constants are all equal. Therefore we can use independent functional group kinetics,[38] in which the hydrolyzed functional group (SiOH) is the only species that participates in the condensation reaction. If we use C_3 to denote the concentration of (SiOH), then based on the fact that one Si atom is associated with $4(1-\alpha)$ (SiOH) functional groups where $\alpha =$ the siloxane bond conversion, we write the conservation equation, initial and boundary conditions for C_3 as follows:

$$\frac{\partial C_3}{\partial t} - 4(1-\alpha)D_2\frac{\partial^2 C_2}{\partial z^2} = -k_{00}C_3^2. \tag{26}$$

Initial conditions:

$$C_3(0,z) = C_{3,0} = 4C_{2,0} \tag{27}$$

Boundary conditions:

$$\text{At substrate } (z=0): \quad D_3\frac{\partial C_3}{\partial z} = 0 \tag{28}$$

At free surface ($z = H(t)$):

$$\frac{\partial C_3}{\partial z} = -4(1-\alpha)\frac{\hat{V}_1}{\hat{V}_2}\frac{\partial C_1}{\partial z} \tag{29}$$

Dimensionless Variables and Simulation Procedure. The following dimensionless variables are defined to solve the transport equations numerically:

$$\eta = z/H(t), \quad h = H(t)/H_0, \quad c_i = C_i/C_{1,0}, \quad q_i = Q_i^C/C_0, \quad \tau = \frac{D_1}{H_0^2}t. \tag{30}$$

Using the dimensionless variable η, the region in which diffusion occurs is always from $\eta = 0$ to $\eta = 1$. In other words, the physical moving domain is mapped onto a fixed domain, and we do not need to modify the spatial grid during the simulation. Meanwhile, a pseudoconvective term is produced by this Landau transformation[57] in the diffusion equation.[56] For example, the dimensionless form of the equation for the solvent now is

$$\frac{\partial c_1}{\partial \tau} - \frac{\eta}{h}\times\frac{dh}{d\tau}\times\frac{\partial c_1}{\partial \eta} - \frac{1}{h^2}\frac{\partial^2 c_1}{\partial \eta^2} = 0. \tag{31}$$

We can see that this pseudoconvective term is proportional to the free surface velocity $\frac{dh}{d\tau}$.

This set of dimensionless equations is numerically solved using the explicit centered finite difference method (FDM). We discretize the whole domain into a number of thin slices, each with a fixed thickness $\Delta\eta$ (here $\Delta\eta = 0.04$). For the solution, the time interval Δt is equal to the time interval between reactions estimated from the DMC simulation, which is on the order of 10^{-9} to 10^{-11}. The stability of the FDM for partial differential equations can be evaluated from the ratio $\Delta t/(\Delta\eta)^2$, which in our case is on the order of 10^{-6} to 10^{-8}. This value is much smaller than the value required for numerical stability, which is 0.5. Therefore, using time intervals from the DMC model is feasible and ensures the stability of our continuum model. As mentioned above, this time interval from the DMC model serves as one "handshake" with the continuum model. At each finite difference step, we use the concentrations, film thickness, surface velocity, and Robin boundary condition at the surface from the previous time step to complete the calculation.

Tracking a Sol Particle. As we mentioned before, the entire DMC simulation is treated as a particle of sol whose position and composition are tracked in the continuum model (as shown in Figure 1), which provides an important link between the components of our multiscale model. We perform the tracking using linear interpolation. Similar to the film thickness calculation Eq. 25, the change of particle position $H_p(t)$ can be expressed as follows:

$$\frac{dH_p(t)}{dt} = \hat{V}_1 \times D_1\frac{\partial C_1}{\partial z}\bigg|_{H_p}. \tag{32}$$

From the value of particle position at the previous step of the calculation, we can determine the finite difference slice

where the particle is located. Then we are able to estimate the approximate value of concentration gradient in that interval (between slice $(m-1)$ and slice m, Eq. 33) and continue to calculate the composition (Eq. 34) and position (Eq. 35) of the particle (expressed in dimensionless form):

$$\frac{\partial c_i}{\partial \eta} \approx \frac{c_{i,m} - c_{i,(m-1)}}{\Delta\eta}, \quad \frac{\partial q_i}{\partial \eta} \approx \frac{q_{i,m} - q_{i,(m-1)}}{\Delta\eta}, \tag{33}$$

$$c_{p_i} = c_{i,m} - \frac{\partial c_i}{\partial \eta} \times (m \times \Delta\eta - h_p),$$

$$c_{q_i} = q_{i,m} - \frac{\partial q_i}{\partial \eta} \times (m \times \Delta\eta - h_p), \tag{34}$$

$$h_p(t+1) = h_p(t) + d\tau \times \frac{1}{h^2} \times \frac{\partial c_1}{\partial \eta} \times C_{1,0}\hat{V}_1, \tag{35}$$

where c_{p_i} ($i = 1$, 2, or 3) is the dimensionless concentration of solvent, total silicon sites or (SiOH) groups at the particle position, and c_{q_i} is the dimensionless concentration of silicon sites with i siloxane bonds at the particle position. Using the calculated concentrations within this tracked particle (Eq. 34), we can then determine the conversion and total silicon site concentration in the continuum model (Eqs. 36–40). This total silicon site concentration C_{si} provided by the continuum model is then supplied to the DMC routine to choose the next reaction and calculate the time interval of the next DMC step (Eq. 10), which is the second "handshake" between the continuum model and the DMC model. The equations we use to calculate conversion and overall silicon concentration from the integrated concentrations for the two polymerization cases are presented below:

$$\text{Ideal case}: \quad \alpha = 1 - \frac{c_{p_3}}{4 \times c_{p_2}}, \quad C_{\text{Si}} = c_{p_2} \times C_{1,0} \tag{36}$$

FSSE case :

$$a = c_{q_1} + 2 \times c_{q_2} + 3 \times c_{q_3} + 4 \times c_{q_4}, (\text{reacted [SiOH]}) \tag{37}$$

$$b = 4 \times c_{q_0} + 3 \times c_{q_1} + 2 \times c_{q_2} + c_{q_3}, (\text{remaining [SiOH]}) \tag{38}$$

$$C_{\text{Si}} = c_{p_2} \times C_{1,0} = (a+b) \times C_{1,0}/4, \tag{39}$$

$$\alpha = 1 - \frac{b}{4 \times c_{p_2}} = \frac{a}{4 \times c_{p_2}} = \frac{a}{a+b}. \tag{40}$$

Using these expressions, we can compare the conversions and site distributions (for the FSSE case) with those obtained from the DMC model to validate the implementation of this multiscale model. Note that the DMC model still contains a significant amount of information about the polymer structure distribution that is not available from a continuum kinetics approach.

Results and Discussion

The modeling equations described above were used to perform calculations for varying initial sol positions and process parameters using with a set of PCs with AMD Athlon processors. In our modeling, we focus on the effects of two important dimensionless parameters, *Bi* and *Da* (Eq. 41) to understand how process parameters affect the evolution of sol-gel silica films. *Bi* is the Biot number, which is the ratio of external mass transfer resistance to the internal diffusion resistance, and can be thought of as a dimensionless mass transfer time. *Da* is the Damköhler number, which is the ratio of reaction rate to diffusion rate, and can be thought of as a dimensionless reaction time. In the FSSE case, we have different rate coefficients, but we use the first reaction rate coefficient k_{00} as the reference to define the Damköhler number. For a negative FSSE (considered here) k_{00} is the largest rate coefficient.

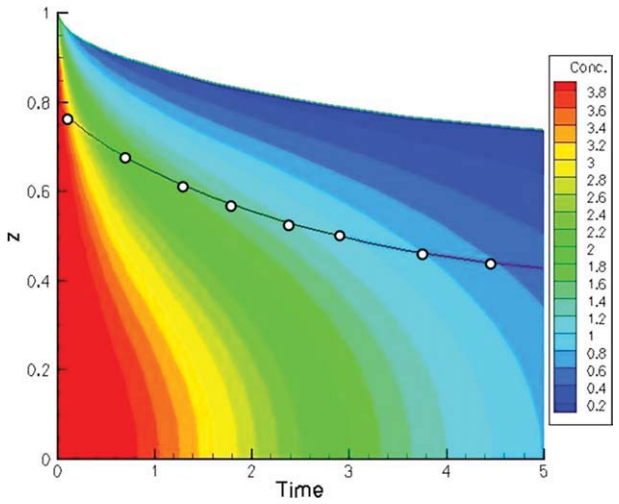

Figure 2. Time-dependent solvent concentration profile for the FSSE case calculated with *Bi* = 506.625, *Da* = 40, H_0 = 1.0, and $H_{p_0} = 0.8H_0$.

[Color figure can be viewed in the online issue, which is available at wileyonlinelibrary.com.]

$$Bi = \frac{k_g H_0 \hat{V}_1}{D_1}, \quad Da = \frac{k_{00} C_{1,0} H_0^2}{D_1}. \tag{41}$$

Note that in the DMC simultation, a natural dimensionless time scale is given by $t^* = k_{00} C_{\text{Si},0} t$, so the FDM and DMC time scales can be related by $t^*/\tau = Da(C_{\text{Si},0}/C_{1,0})$. The ratio of initial concentration used here is $C_{1.0} : C_{2.0} = 4{:}1$, and the value of solvent molar volume is arbitrarily set to 0.1.

Solvent concentration profile

Figure 2 displays an example of the time-dependent solvent concentration profile in the films which is calculated by the continuum model for the FSSE case. The red curve with points shows the change of the tracked sol particle position for this example. As expected, the film thickness, solvent concentration and particle position all drop as the gel film dries. This suggests that the transport equations are being correctly handled. Simplified cases of the transport with boundary conditions amenable to symbolic solutions (for instance, drying without reaction and with constant rate of evaporation at the free surface) were also tested and found to agree well with the numerical solutions, thus confirming the accuracy of our implementation of the finite difference method.

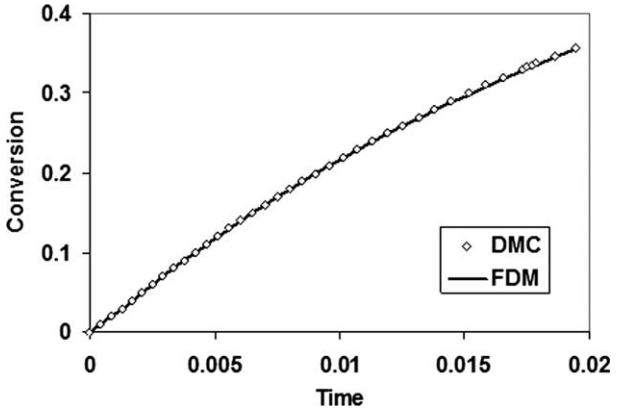

Figure 3. Comparison of the conversion predicted by both the DMC and continuum models for the ideal case.

$Bi = 1013.25$, $Da = 2.0$, and $Hp_0 = 0.9H_0$.

Conversion and site distribution

Because we can calculate the conversion and site distributions (for the FSSE case) as functions of time using continuum equations in addition to the DMC model, the validity of this multiscale model is tested by comparing the continuum results to the DMC results, as presented for two examples in Figures 3 and 4. In both cases shown, the results are terminated shortly after a gel forms (indicated by either the apparent divergence of DP_w or a peak in rDP_w, as discussed earlier). The ability to validate the DMC approach is one of the advantages of developing the multiscale model for relatively simple polymerization kinetics. For both ideal and FSSE cases, the conversions calculated by the two methods agree exactly, as shown in Figures 3 and 4. In addition, the site distributions calculated by the continuum and DMC methods for the FSSE case agree well, as shown in Figure 5. The good agreement found between the continuum kinetics and the DMC results prove the validity of our implementation of the coupled DMC/continuum method. In addition, this set of figures shows that, as expected, because the rate coefficients

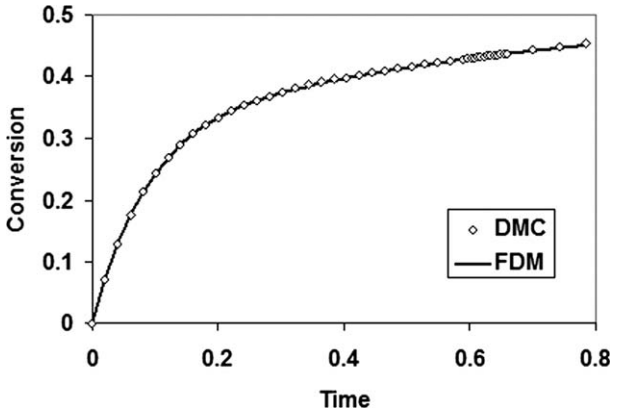

Figure 4. Comparison of the conversion predicted by both the DMC and continuum models for the FSSE case.

$Bi = 506.625$, $Da = 40$, and $Hp_0 = 0.8H_0$.

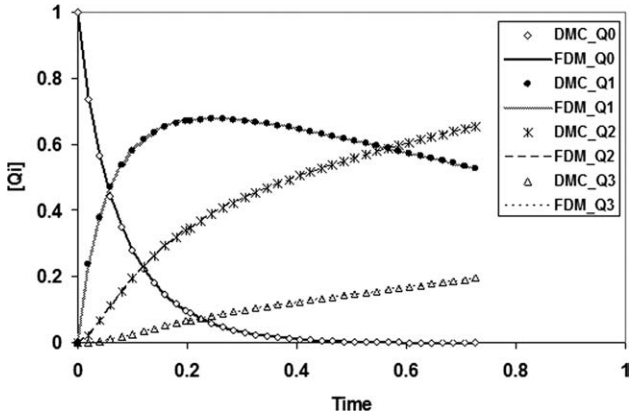

Figure 5. Site distributions predicted by both the DMC and continuum models for the FSSE case.

$Bi = 506.625$, $Da = 40$, and $Hp_0 = 0.8H_0$.

drop in the FSSE case, the rate of the condensation reactions decreases significantly compared with the ideal case, and because of the structure of the resulting polymers, gelation occurs at a larger conversion and therefore at a much later time.

Competition between drying and gelation

There are three main types of qualitative drying and gelation phenomena in the drying process of a sol-gel film, as originally defined by Cairncross et al.[38]: Drying before gelation, gelation before drying and literal skinning. Literal skinning means that, when the film surface has formed a solid gel network, the solution inside the film is still liquid, which may lead to coating defects such as wrinkling and possibly cracking.[38] The competition between drying and gelation determines the type of phenomenon, and this competition is dictated by the values of Biot number and Damköhler number. We define these three types of phenomena by comparing the values of gel time with drying time, according to the definitions of Cairncross et al.[38] The gel time is the time at which the DMC simulation of the sol particle reaches the gel point (see later). The drying time is calculated by integrating the solvent content throughout the coating and finding the point at which only 1% of the initial solvent content is left.[38] The definitions of the three types of phenomena are as follows:

- drying before gelation: dry_t<gel_tb,
- gelation before drying: gel_tb<10% × dry_t,
- literal skinning: $\frac{\text{gel\_tb}-\text{gel\_ts}}{\text{dry\_}t} \geq 0.1$,

where dry_t denotes the drying time, gel_tb is the gel time at the base of the coating, and gel_ts is the gel time at the coating surface. The gel time varies throughout the film because of concentration gradients due to the solvent evaporation, an example of which is illustrated in Figure 2.

Figure 6 displays the DMC-generated values of DP_w as a function of time for tracked particles starting from different positions in the film and for one particular set of process parameters ($Bi = 1013.25$ and $Da = 0.4$). It is obvious that DP_w increases much more quickly at the film surface than inside the film, and that means there is a time lag of gelation between the film surface and base. At any point in the film,

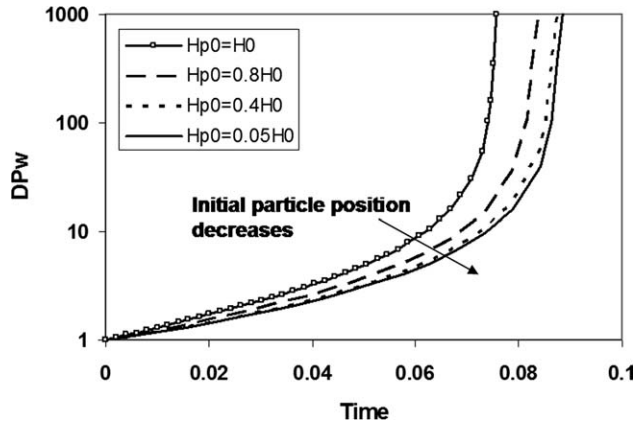

Figure 6. DP_w as a function of time for tracked sol particle starting at different positions in the film for the ideal literal skinning case.

$Bi = 1013.25$ and $Da = 0.4$.

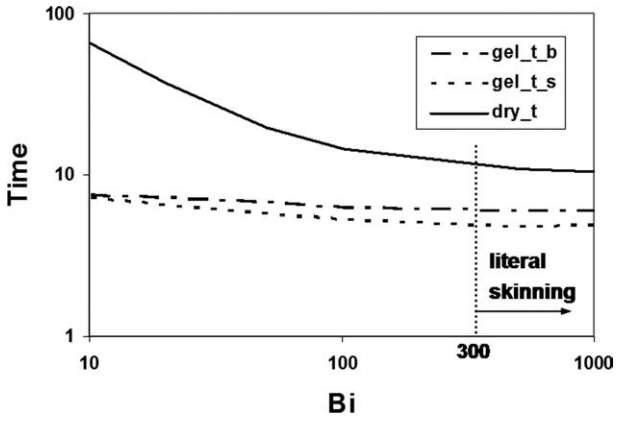

Figure 8. Gelation and drying times as a function of *Bi* for the FSSE case with constant *Da* = 4.0.

When $Bi \geq 300$, literal skinning occurs in this set of simulations.

gelation is defined by the point where DP_w appears to diverge (as discussed above).

The effects of process parameters *Bi* and *Da* on the gelation and drying time for the ideal and FSSE cases are illustrated with examples in Figures 7 and 8. Figure 7 shows the effect of varying *Da* number with constant *Bi* (equal to 1013.25) in the ideal case. In this case, the drying time remains constant and gel time drops considerably as *Da* increases. At this high *Bi*, drying before gelation, literal skinning and gelation before drying appears in turn with increasing reaction rates, which means that the type of phenomenon depend only on *Da* when the value of *Bi* is high.

Figure 8 shows another representative result: the gelation and drying times at various *Bi* values for the FSSE case. With constant $Da = 4.0$, gelation is always faster than drying. At low *Bi* ($Bi \leq 10$), the difference of the gel time between the coating surface and base of the film is so small that we conclude that the coating gels uniformly. However, the gel time lag between surface and base increases with increasing *Bi*, and literal skinning is predicted to occur when *Bi* is equal to or larger than 300 for the FSSE polycondensation results illustrated in Figure 8.

Gelation regime maps

One could continue generating curves analogous to Figures 7 and 8 for other cases, but the competition between drying and gelation as a function *Bi* and *Da* can be most clearly visualized using gelation regime maps, which define the boundaries between gelation before drying, drying before gelation, and literal skinning.[38] Figures 9 and 10 present these maps determined by our multiscale DMC/finite difference modeling for the ideal and FSSE cases, respectively. The curves in the figures are the approximate boundaries between regions (as defined earlier) and the points are the exact conditions at which transitions between phenomenon types were observed,[38] averaged over five repeated simulations. At low *Da*, the coating dries before it gels and at high

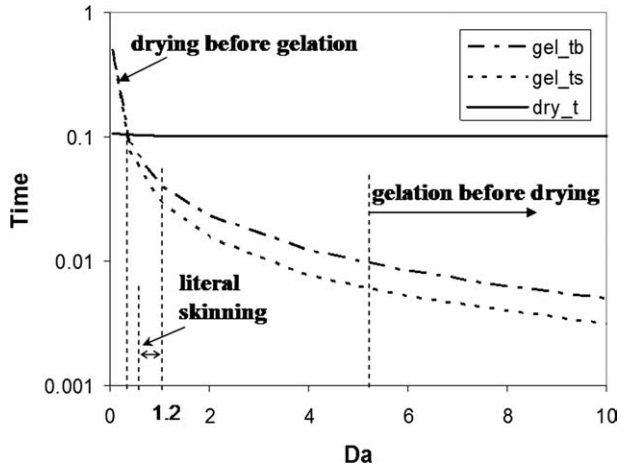

Figure 7. Gelation and drying times as a function of *Da* for the ideal case with constant *Bi* = 1013.25.

Dependence of the type of coating phenomenon on *Da* is indicated.

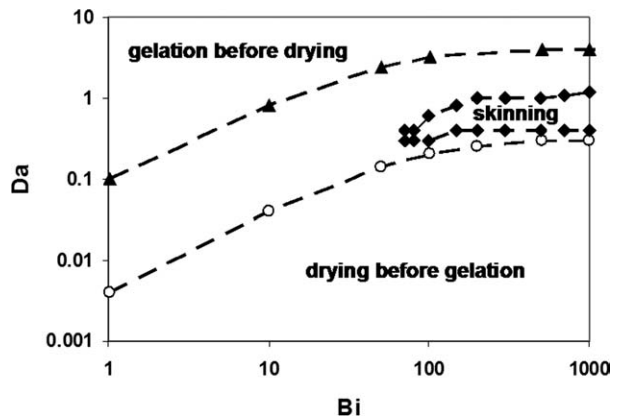

Figure 9. Gelation regime map for the ideal polycondensation case.

Points are the average values of five repeated simulations. Dashed lines are the approximate boundaries of each region.

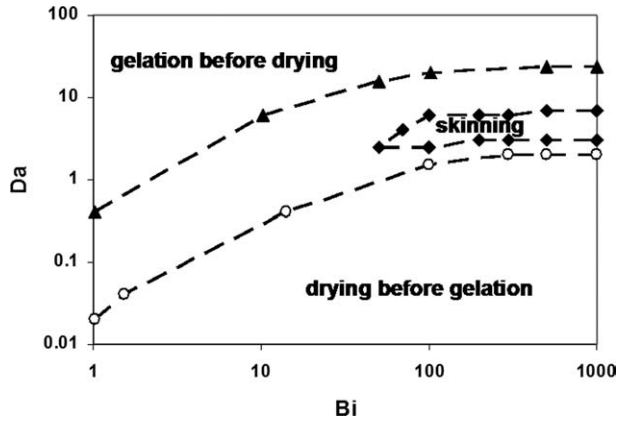

Figure 10. Gelation regime map for the FSSE polycondensation case.

Points are the average values of five repeated simulations. Dashed lines are the approximate boundaries of each region.

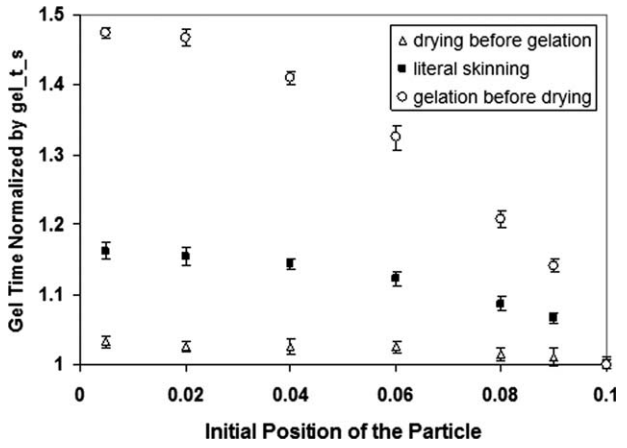

Figure 11. Normalized gel time as a function of initial particle position of the sol calculated by our multiscale model for the ideal case with *Bi* = 1013.25.

Points are the average values of five repeated simulations. The gel time is normalized by the value at the surface. For Drying before gelation, $Da = 0.06$ and gel_ts = 0.506; Literal skinning, $Da = 0.4$ and gel_ts = 0.0765; Gelation before drying, $Da = 2.0$ and gel_ts = 0.0156.

Da, the gelation reaction rates are much quicker than the drying rate. With high *Bi*, literal skinning occurs between the regions of "drying before gelation" and "gelation before drying". The maps are similar for the ideal and FSSE cases, except that with FSSE, all three regions are shifted towards higher *Da*. These results are consistent with the findings of Cairncross et al.,[38] but they used an approximate kinetic-recursive model with reduced accuracy for FSSE modeling. There are also quantitative differences in the positions of the boundaries in the FSSE case because a different matrix of rate coefficients was assumed. Although the kinetic-recursive model can be solved much more quickly than the DMC model, discrepancies appear for certain cases of strong FSSE,[21] and a statistical approach is not capable of correctly modeling the high degree of cyclization found in real sol-gel polymerization[19,22,45] (to be discussed in future contributions from our group).

Relationship between gel time and initial particle position

To gain more insight into the effects of the FSSE on film uniformity, we further investigate the relationship between gel time and initial particle position for the three qualitative types of sol-gel coating phenomena, as shown in Figures 11 and 12. Representative points from the gelation regime maps are shown. According to the maps, we can observe all three types of phenomena by setting *Bi* to a high value and varying *Da*. In order to compare these three types phenomena easily, all of the gel time values are normalized by the one at the surface. With fixed *Bi*, gel times are, of course, longest when "drying before gelation" is found and smallest when "gelation before drying" is found. The multiscale model predicts that the gel time gradient is much more severe when "gelation before drying" is observed than with "drying before gelation". This suggests that, when the coating dries completely as a liquid (drying before gelation) the gel time lag is small and defects are not likely to appear due to formation of a gel layer at the film surface, and when the coating gels before it is dry, the difference of gel time is more visible and likely to induce defects. Regardless of the rate of drying, drying before gelation is best achieved by reducing the rate of condensation relative to the rate of diffusion of solvent. In sol–gel systems, this can be accomplished by working near the minimum condensation rate which occurs at a pH of ~2.[18] Gel times for the FSSE case simulations are longer than those of ideal case, indicating again that gelation is delayed compared with the ideal case, as we mentioned earlier. Also, the gradients in gel time are more severe with a negative FSSE than those found in the ideal case, suggesting that nonideal polymerization may worsen the formation of coating defects in sol–gel systems.

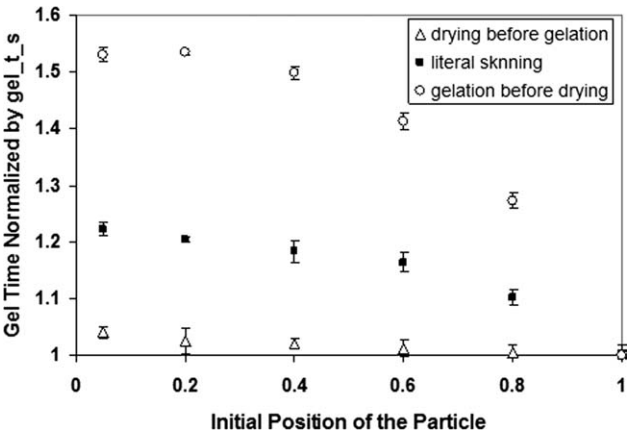

Figure 12. Normalized gel time as a function of initial particle position of the sol calculated by our multiscale model for the FSSE case with *Bi* = 506.625.

Points are the average values of five repeated simulations. The gel time is normalized by the value at the surface. For Drying before gelation, $Da = 0.4$ and gel_ts = 47.9; Literal skinning, $Da = 4.0$ and gel_ts = 4.97; Gelation before drying, $Da = 40.0$ and gel_ts = 0.514.

Conclusions

The proposed multiscale model for the drying process of sol-gel coatings couples molecular to macroscopic phenomena by combining dynamic Monte Carlo simulations and the finite difference method. For the (relatively) simple cases studied here, continuum equations are formulated for the overall extents of reaction, and the results agree well with the multiscale DMC/FDM model. In the continuum model, the entire DMC simulation is treated as a particle of sol whose position and composition are tracked using a diffusion/evaporation finite difference calculation. Therefore, the total silicon concentration provided by the continuum model serves as one "handshake" with the DMC model. The second "handshake" between the models is the time interval from the DMC simulation, which is also used as the time interval for the continuum model. By simulating swarms of particles starting from different positions in the film, we observe the effects of varying process parameters on the competition between drying and gelation, thereby predicting different drying/gelation phenomena and the occurrence of gradients of concentration and gelation in the films. Conditions are found which can lead to the formation of a gel skin near the top surface of the film for both ideal polycondensation and a FSSE consistent with NMR studies of silane polycondensation.

The establishment of this multiscale model approach is our first step to building a more physically accurate model of the sol-gel coating processes with drying and curing. Further work is needed to improve the realism of the polymerization model, the most important and obvious aspect of which is to add cyclization to the model[19,22] and see its effects on gelation regime maps and structural gradients. We expect that refining the polymerization model within the context of this multiscale simulation approach will allow better prediction of the formation of structure gradients in sol-gel derived ceramics and other nonideal multifunctional polycondensation products, which will help in developing coating procedures to reduce coating defects.

Acknowledgments

This work is supported by the U.S. Department of Energy under grant numbers DE-FG02-03ER46033 and DE-FG02-07ER46375.

Notation

Bi = Biot number
C = concentration
c = dimensionless concentration
c_p = dimensionless concentration at the particle position
c_q = dimensionless concentration of silicon site at the particle position
D = diffusion coefficient
Da = Damköhler number
DP_w = the weight-averaged degree of polymerization
dry_t = the drying time
dt = time interval in FDM
f = the functionality of the monomer
gel_tb = the gel time at the coating base
gel_ts = the gel time at the coating surface
h = the dimensionless film thickness
h_p = the dimensionless particle position
$H(t)$ = the instantaneous film thickness
H_p = the particle/sol position in the film
H_0 = the initial film thickness
i = number of siloxane bonds
j = number of siloxane bonds
k_{ij} = the rate constant of bimolecular polycondensation
k_g = mass transfer coefficient of solvent
L = molecules size
L_{max} = the size of the largest molecule in the population
N = the total numbers of sites considered in DMC simulation
N_A = the Avogadro number (6.022E + 23 mol^{-1})
N_{mol} = the number of molecules
N_{Q_i} = the number of silicon sites Q_i
P_{ij} = the probabilities of condensation reactions
Q_i = the tetrafunctional silicon site with i siloxane bonds
Q_i^C = the concentration of a tetrafunctional silicon site with i siloxane bonds in the continuum model
q_i = dimensionless concentration of Q_i^C species in the continuum model
r = the random number from (0, 1)
$r\mathrm{DP}_w$ = the reduced weight-averaged degree of polymerization
R_{ij}^{bimol} = the reaction rate of bimolecular reaction
R_Q^C = the net rate for creation of each type of site through reaction in the continuum model
S_t = the total number of DMC steps
Δt = time interval calculated by MC method
V = the volume of the DMC simulation
v^s = the free surface velocity
$\hat{V}$ = molar volume
y_1^s = the molar fraction of solvent at the surface in the gas phase
y_1^∞ = the molar fraction of solvent far away in the gas phase
z = distance from the bottom
α = conversion
η = dimensionless distance from the coating bottom
τ = dimensionless time
χ = hydrolysis extent

Subscripts

With C: 0 = initial concentration
1 = solvent
2 = total silicon
3 = (SiOH) functional group
With Q^C/q: i = number of siloxane bonds attached to the silicon site

Literature Cited

1. Sanchez C, Boissiere C, Grosso D, Laberty C, Nicole L. Design, synthesis, and properties of inorganic and hybrid thin films having periodically organized nanoporosity. *Chem Mater*. 2008;20:715–720.
2. Stein A, Melde BJ, Schroden RC. Hybrid inorganic-organic mesoporous silicates-nanoscopic reactors coming of age. *Adv Mater*. 2000; 12:1412–1417.
3. Brinker CJ, Dunphy DR. Morphological control of surfactant-templated metal oxide films. *Curr Opin Colloid Interface Sci*. 2006;11: 126–132.
4. Kambhampati DK, Jakob TAM, Robertson JW, Cai M, Pemberton JE, Knoll W. Novel silicon dioxide sol-gel films for potential sensor applications: a surface plasmon resonance study. *Langmuir*. 2001;17: 1169–1175.
5. Anitha K, Mohan SV, Reddy SJ. Development of acetylcholinesterase silica sol-gel immobilized biosensor. An application towards oxydemeton methyl detection. *Biosens Bioelectron*. 2004;20:848–856.
6. Martucci A, Buso D, Monte MD, Guglielmi M, Cantalini C, Sada C. Nanostructured sol-gel silica thin films doped with NiO and SnO_2 for gas sensing applications. *J Mater Chem*. 2004;14:2889–2895.
7. Buso D, Guglielmi M, Martucci A, Cantalini C, Post ML, Hache A. Porous sol gel silica films doped with crystalline NiO nanoparticles for gas sensing applications. *J Sol-Gel Sci Technol*. 2006;40:299–308.
8. Palaniappan A, Su X, Tay FEH. Functionalized mesoporous silica films for gas sensing applications. *J Electroceramics*. 2006;16:503–505.

9. Di JW, Cheng JJ, Xu QA, Zheng HI, Zhuang JY, Sun YB, Wang KY, Mo XY, Bi SP. Direct electrochemistry of lactate dehydrogenase immobilized on silica sol-gel modified gold electrode and its application. *Biosens Bioelectron*. 2007;23:682–687.
10. Musat V, Fortunato E, Botelho do Rego AM, Monteiro R. Sol-gel cobalt oxide-silica nanocomposite thin films for gas sensing applications. *Thin Solid Films*. 2008;516:1499–1502.
11. Konjhodzic D, Bretinger H, Marlow F. Structure and properties of low-n mesoporous silica films for optical applications. *Thin Solid Films*. 2006;495:333–337.
12. Teyssier J, Le Dantec R, Galez C, Mugnier Y, Bouillot J, Plenet J-C. LiIO3/SiO2 nanocomposite for quadratic non-linear optical applications. *J Non-Cryst Solids*. 2004;341:152–156.
13. Molenkamp WC, Watanabe M, Miyata H, Tolbert SH. Highly polarized luminescence from optical quality films of a semiconducting polymer aligned within oriented mesoporous silica. *J Am Chem Soc*. 2004;126:4476–4477.
14. Blanc D, Zhang W, Massard C, Mugnier J. Synthesis and characterisation of tantalum-incorporating silica hybrid sol-gel thin films for optical applications. *Opt Mater (Amsterdam, Netherlands)*. 2006;28:331–335.
15. Olding T, Sayer M, Barrow D. Ceramic sol-gel composite coatings for electrical insulation. *Thin Solid Films*. 2001;398–399:581–586.
16. Nostell P, Roos A, Karlsson B. Optical and mechanical properties of sol-gel antireflective films for solar energy applications. *Thin Solid Films*. 1999;351:170–175.
17. Brinker CJ, Lu YF, Sellinger A, Fan HY. Evaporation-induced self-assembly: nanostructures made easy. *Adv Mater*. 1999;11:579–585.
18. Brinker CJ, Scherer GW. *Sol-Gel Science: The Physics and Chemistry of Sol-Gel Processing*. San Diego, CA: Academic Press, 1990.
19. Rankin SE, Kasehagen LJ, McCormick AV, Macosko CW. Dynamic Monte Carlo simulation of gelation with extensive cyclization. *Macromolecules*. 2000;33:7639–7648.
20. Bailey JK, Macosko CW, Mecartney ML. Modeling the gelation of silicon alkoxides. *J Non-Cryst Solids*. 1990;125:208–223.
21. Kasehagen LJ, Rankin SE, McCormick AV, Macosko CW. Modeling of first shell substitution effects and preferred cyclization in sol-gel polymerization. *Macromolecules*. 1997;30:3921–3929.
22. Šefčlk J, Rankin SE. Monte Carlo simulations of size and structure of gel precursors in silica polycondensation. *J Phys Chem B*. 2003;107:52–60.
23. Cerro RL, Scriven LE. Rapid free surface film flows. An integral approach. *Ind Eng Chem Fundam*. 1980;19:40–50.
24. Cairncross RA. Modeling drying during low-speed coating of porous and continuous films. *IS&T's Annu Conf*. 1997;50:554–558.
25. Verros GD, Malamataris NA. Finite element analysis of polymeric membrane and coating formation by solvent evaporation. *Comput Mechan*. 2001;27:332–340.
26. Réglat O, Labrie R, Tanguy PA. A new free surface model for the dip coating process. *J Comput Phys*. 1993;109:238–246.
27. Blandin HP, David JC, Vergnaud JM, Illien JP, Malizewicz M. Modelling of drying of coatings: effect of the thickness, temperature and concentration of solvent. *Prog Org Coat*. 1987;15:163–172.
28. Alsoy S, Duda JL. Drying of solvent coated polymer films. *Drying Technol*. 1998;16:15–44.
29. Lou HH, Huang YL. Integrated modeling and simulation for improved reactive drying of clearcoat. *Ind Eng Chem Res*. 2000;39:500–507.
30. Vrentas JS, Vrentas CM. Drying of solvent-coated polymer films. *J Polym Sci Part B: Polym Phys*. 1994;32:187–194.
31. Karakasidis TE, Charitidis CA. Multiscale modeling in nanomaterials science. *Mater Sci Eng C*. 2007;27:1082–1089.
32. Praprotnik M, Delle Site L, Kremer K. Multiscale simulation of soft matter: From scale bridging to adaptive resolution. *Annu Rev Phys Chem*. 2008;59:545–571.
33. Jensen KF, Rodgers ST, Venkataramani R. Multiscale modeling of thin film growth. *Curr Opin Solid State Mater Sci*. 1998;3:562–569.
34. Dollet A. Multiscale modeling of CVD film growth—a review of recent works. *Surface Coat Technol*. 2004;177:245–251.
35. Drews TO, Webb EG, Ma DL, Alameda J, Braatz RD, Alkire RC. Coupled mesoscale—continuum simulations of copper electrodeposition in a trench. *AIChE J*. 2004;50:226–240.
36. Li XH, Drews TO, Rusli E, Xue F, He Y, Braatz R, Alkire R. Effect of additives on shape evolution during electrodeposition. I. Multiscale simulation with dynamically coupled kinetic Monte Carlo and moving-boundry finite-volume codes. *J Electrochem Soc*. 2007;154:D230–D240.
37. Raimondeau S, Vlachos DG. Recent developments on multiscale, hierarchical modeling of chemical reactors. *Chem Eng J*. 2002;90:3–23.
38. Cairncross RA, Francis LF, Scriven LE. Predicting drying in coatings that react and gel: drying regime maps. *AIChE J*. 1996;42:55–67.
39. Lou Y, Christofides PD. Feedback control of growth rate and surface roughness in thin film growth. *AIChE J*. 2003;49:2099–2113.
40. Flory PJ. Molecular size distribution in three dimensional polymers. *J Am Chem Soc* 1941;63:3083, 3091, 3096.
41. Stockmayer WH. Theory of molecular size distribution and gel formation in branched-chain polymers. *J Chem Phys*. 1943;11:45–55.
42. Stockmayer WH. Theory of molecular size distribution and gel formation in branched polymers. II. General cross linking. *J Chem Phys*. 1944;12:125–131.
43. Fichthorn KA, Weinberg WH. Theoretical foundations of dynamical Monte Carlo simulations. *J Chem Phys*. 1991;95:1090–1096.
44. Ng LV, Thompson P, Sanchez J, Macosko CW, McCormick AV. Formation of Cagelike intermediates from nonrandom cyclization during acid-catalyzed sol-gel polymerization of tetraethyl orthosilicate. *Macromolecules*. 1995;28:6471–6476.
45. Rankin SE, Macosko CW, McCormick AV. Importance of cyclization during the condensation of hydrolyzed alkoxysilanes. *Chem Mater*. 1998;10:2037–2040.
46. Assink RA, Kay BD. Sol-gel kinetics. I. Functional group kinetics. *J Non-Cryst Solids*. 1988;99:359–370.
47. Assink RA, Kay BD. The chemical kinetics of silicate sol-gels: functional group kinetics of tetraethoxysilane. *Colloids Surfaces A*. 1993;74:1–5.
48. Kay BD, Assink RA. Sol-gel kinetics. II. Chemical speciation modeling. *J Non-Cryst Solids*. 1988;104:112–122.
49. Sanchez J, Rankin SE, McCormick AV. 29Si NMR kinetic study of tetraethoxysilane and ethyl-substituted ethoxysilane polymerization in acidic conditions. *Ind Eng Chem Res*. 1996;35:117–129.
50. Rankin SE, Macosko CW, McCormick AV. Sol-gel polycondensation kinetic modeling: methylethoxysilanes. *AIChE J*. 1998;44:1141–1156.
51. Rankin SE, Sefcik J, McCormick AV. Similarities in the hydrolysis pseudoequilibrium behavior of methyl-substituted ethoxysilanes. *Ind Eng Chem Res*. 1999;38:3191–3198.
52. Rankin SE, McCormick AV. Hydrolysis pseudoequilibrium: challenges and opportunities to sol-gel silicate kinetics. *Chem Eng Sci*. 2000;55:1955–1967.
53. Pouxviel JC, Boilot JP. Kinetic simulations and mechanisms of the sol-gel polymerization. *J Non-Cryst Solids*. 1987;94:374–386.
54. Gillespie DT. A general method for numerically simulating the stochastic time evolution of coupled chemical reactions. *J Comput Phys*. 1976;22:403–434.
55. Hendrickson RC, Gupta AM, Macosko CW. Sol-Gel polymerization: Monte Carlo simulation of substitution effects. *Comput Polym Sci*. 1994;4:53–65.
56. Guerrier B, Bouchard C, Allain C, Bénard C. Drying kinetics of polymer films. *AIChE J*. 1998;44:791–798.
57. Crank J. *Free and Moving Boundary Problems*: Clarendon Press: Oxford, 1988.

Manuscript received July 16, 2009, revision received Dec. 29, 2009, and final revision received Feb. 3, 2010.